

Supplementary Materials for
**Generation and multiomic profiling of a *TP53/CDKN2A* double-knockout
gastroesophageal junction organoid model**

Hua Zhao *et al.*

Corresponding author: De-Chen Lin, dechenli@usc.edu; Stephen J. Meltzer, smeltzer@jhmi.edu

Sci. Transl. Med. **14**, eabq6146 (2022)
DOI: 10.1126/scitranslmed.abq6146

The PDF file includes:

Figs. S1 to S8

Other Supplementary Material for this manuscript includes the following:

Tables S1 to S7

Data files S1 and S2

MDAR Reproducibility Checklist

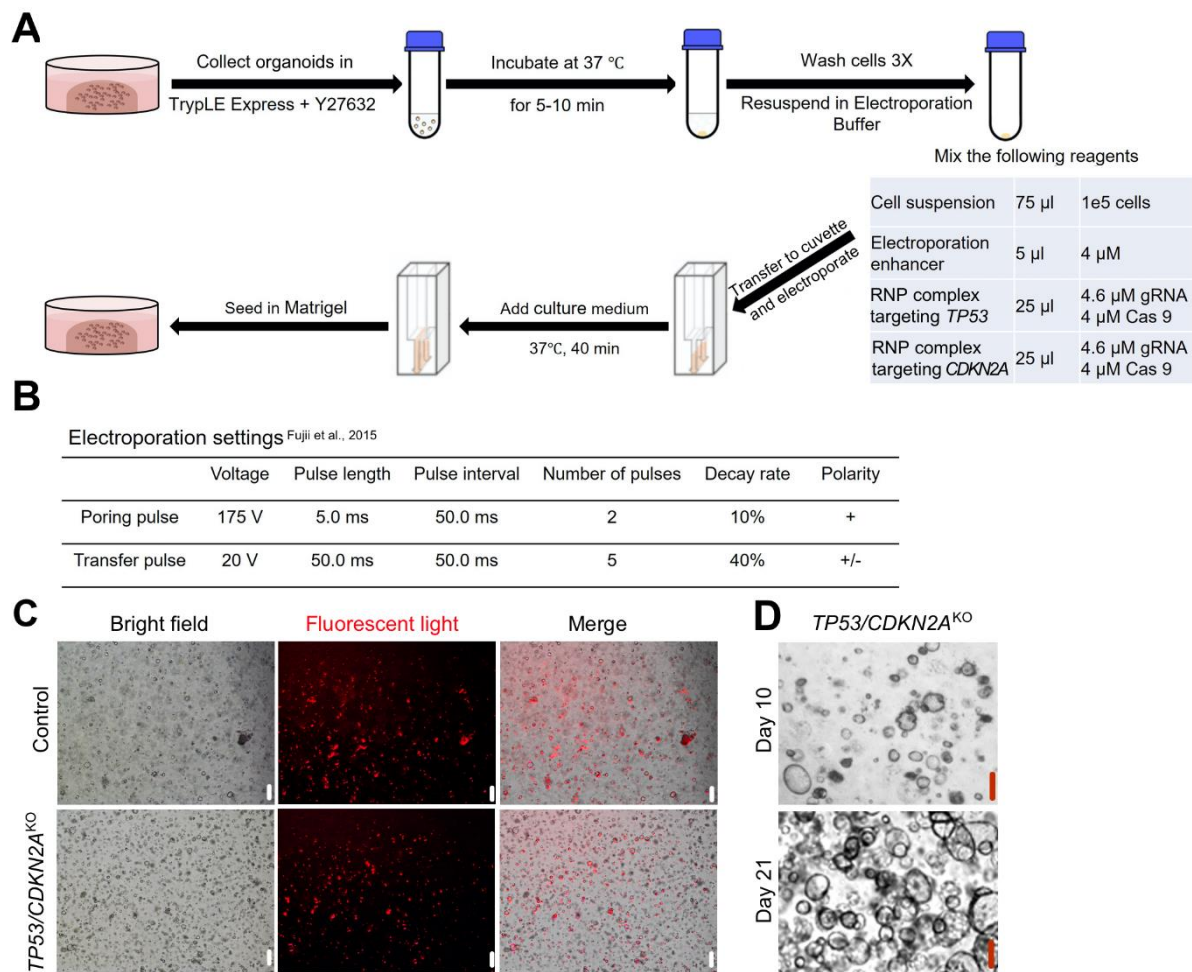


Fig. S1. *TP53/CDKN2A*^{KO} GEJ organoids created by CRISPR-Cas9 genome editing. (A) Electrotransfection preparation workflow and (B) two-step electrotransfection settings. (C) Cas9 nuclease and the negative control or *TP53/CDKN2A*-targeted gRNA complex transfected into GEJ organoids (red fluorescence). (D) Survival and sustained growth of *TP53/CDKN2A*^{KO} GEJ organoids in Nutlin-3a-containing selective medium at day 10 and day 21. Scale bar = 100 μ m.

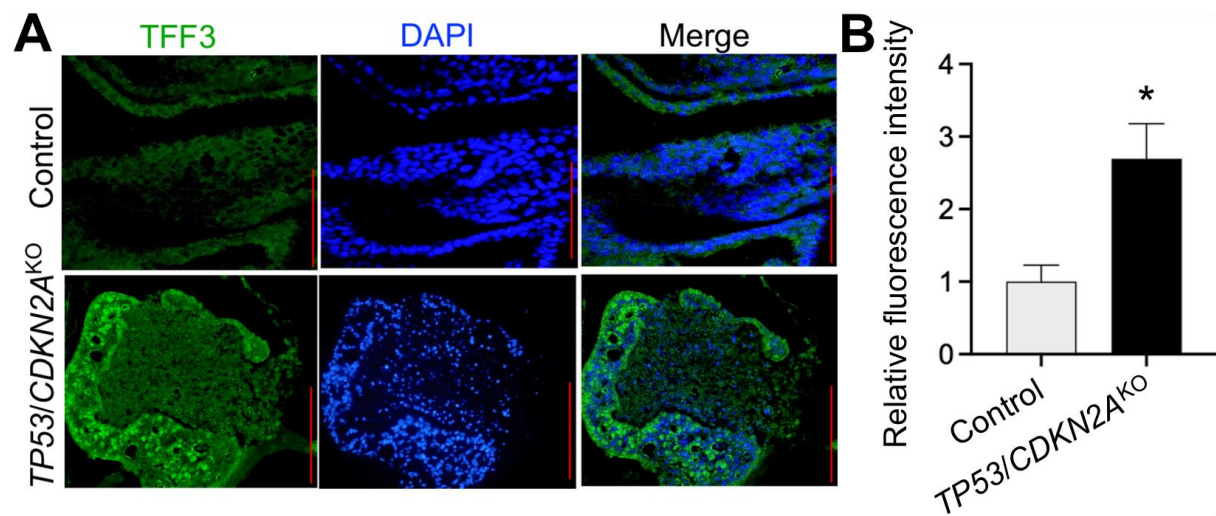


Fig. S2. Double-knockout of *TP53/CDKN2A* promotes TFF3 expression in GEJ

organoids. (A) Representative IF images of TFF3 in normal control and *TP53/CDKN2A*^{KO} GEJ organoids. Scale bar = 100 μ m. (B) Fluorescence intensity was quantified and plotted as fold-changes relative to the control organoids ($n= 3$ biological replicates). Data are presented as mean \pm SD; *, $P < 0.05$ by Student's t-test.

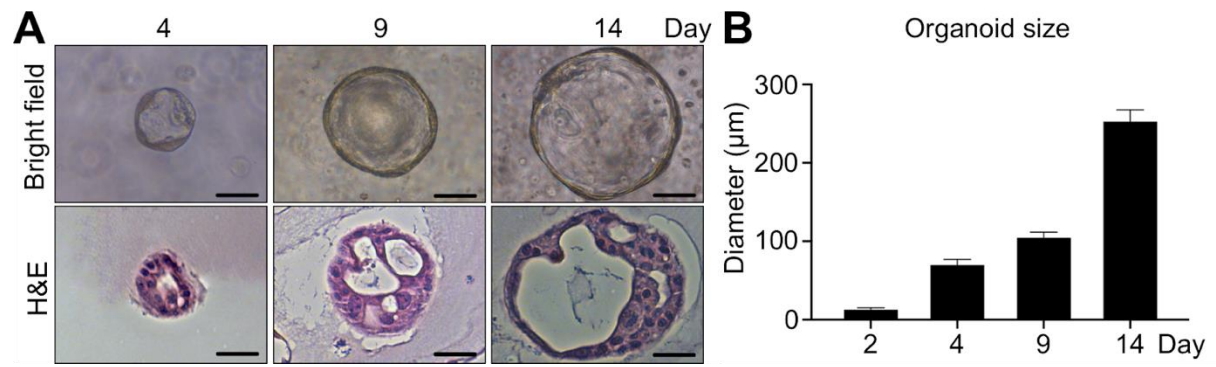


Fig. S3. Characterization of *TP53/CDKN2A*^{KO} GEJ organoid growth. (A) Brightfield (top) and H&E microscopy (bottom) images of *TP53/CDKN2A*^{KO} GEJ organoids at days 4, 9 and 14. Scale bar = 50 μm. (B) Average organoid size was determined by measuring > 10 organoids. Data are represented as mean ± SD; *n*= 4 biologic replicates.

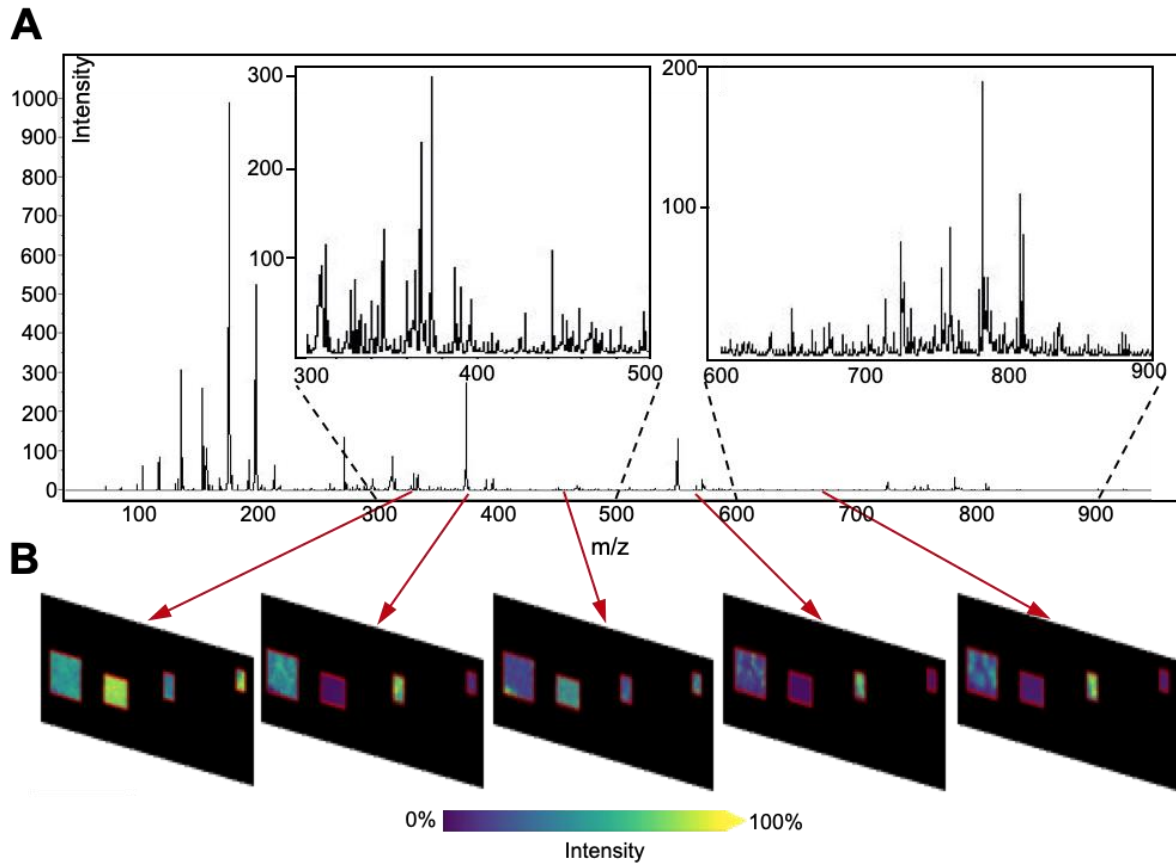


Fig. S4. Overall average lipid spectra and MALDI images of control and *TP53/CDKN2A*^{KO} GEJ organoids. (A) Overall average lipid mass spectra collected from an organoid section. Inset shows detail and complexity of the spectra (typical tissue imaging experiments result in up to thousands of such spectra). (B) Ion images generated from each peak. Each m/z value of interest is displayed as relative intensity.

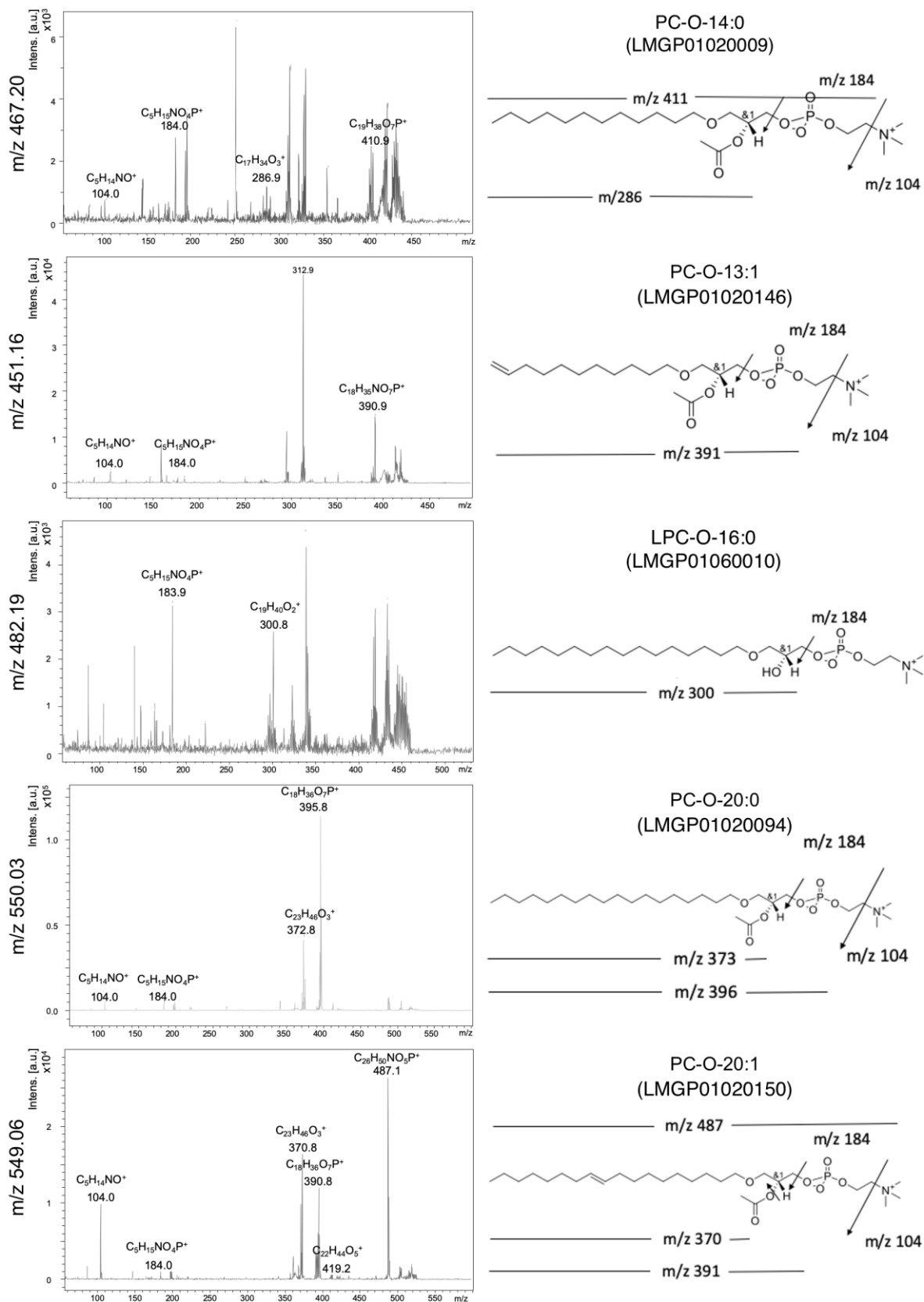


Fig. S5. 4 PTAF lipids and a PTAF lipid precursor identified by MS/MS and fragmentation analysis. Fragmentation MS/MS spectrum (left panel) of PTAF lipids (m/z

467.20, m/z 451.16, m/z 550.03, and m/z 549.06) and PTAF lipid precursor (m/z 482.19). The detected fragments and the enrichment of fragmentation enable identifying the common names, ID, and the chemical structure (right panel) in the Lipid Maps Structure Database.

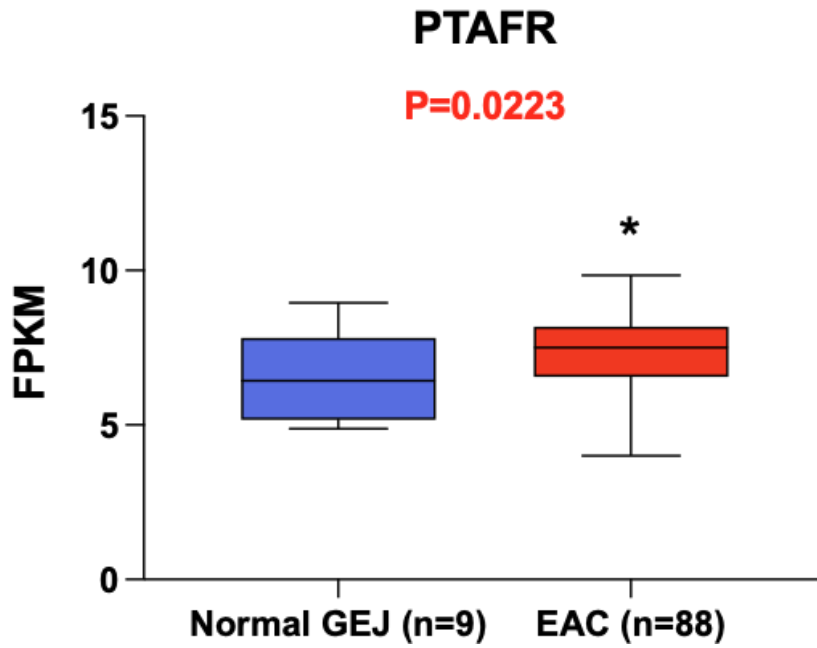


Fig. S6. PTAFR mRNA expression in human normal GEJ versus EAC tissue samples.

Fragments per kilobase of transcript per million mapped fragments (FPKM) data for PTAFR expression from TCGA human normal GEJ ($n=9$) and esophageal adenocarcinoma (EAC) ($n=88$) samples were analyzed. Data are represented as mean \pm SD * $P < 0.05$ by Student's t-test.

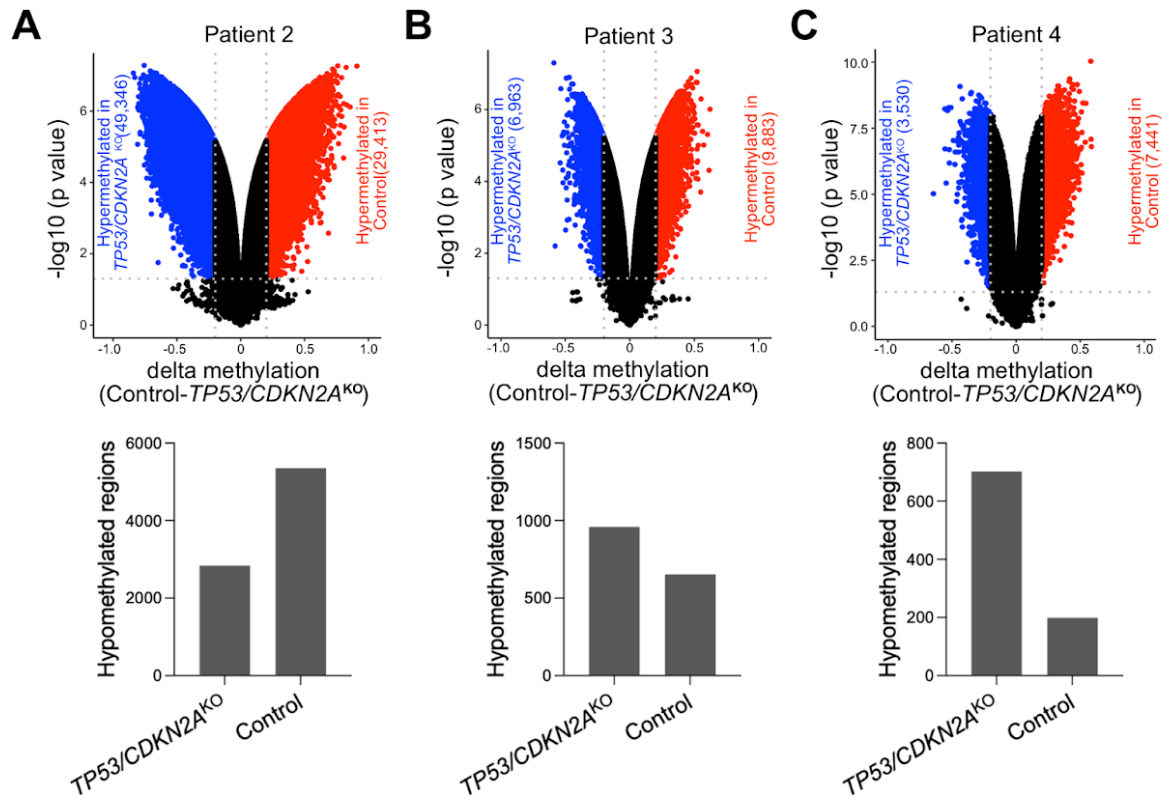


Fig. S7. Global DNA methylation analysis in $TP53/CDKN2A^{KO}$ and control GEJ organoids derived from three different patients. Volcano plots (top) revealed differentially methylated regions (DMRs) **in patient 2 (A), patient 3 (B), and patient 4 (C)**, defined as exceeding a cutoff p-value of < 0.05 and an absolute delta-methylation value of > 0.2 . Hypomethylated regions (bottom) were confirmed in $TP53/CDKN2A^{KO}$ and control organoids, respectively.

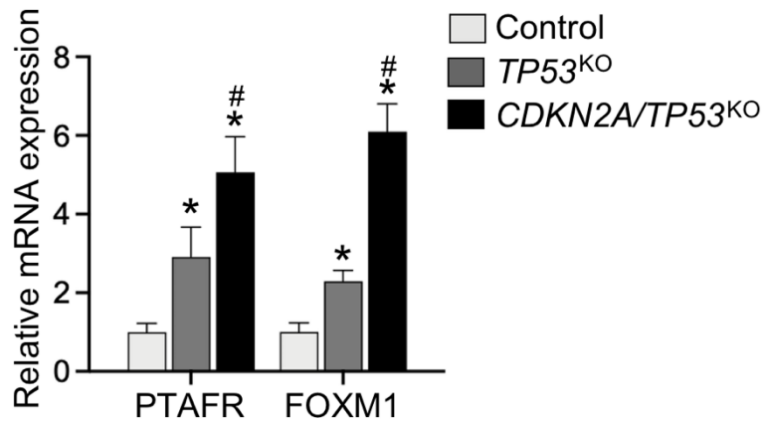


Fig. S8. *CDKN2A* inactivation augments *TP53* inactivation-induced expression of PTAFR and FOXM1 mRNA. qRT-PCR measuring mRNA expression of PTAFR and FOXM1 in control, *TP53*^{KO}, and *TP53/CDKN2A*^{KO} GEJ organoids. Data are presented as mean ± SD, *n*=2 biological replicates. *, *P* < 0.05 versus. Control by ANOVA; #, *P* < 0.05 versus. *TP53*^{KO} by ANOVA.